# Multiphysics Sensor Based on the Nonreciprocal Evanescent Wave in the Magnetized Plasma Cylindrical Photonic Crystals

Jia-Tao Zhang, Si-Si Rao, and Hai-Feng Zhang

**Abstract**—In this paper, a multiphysics quantity sensor is proposed based on a magnetized plasma cylindrical photonic crystals structure which is using the nonreciprocal evanescent wave principle. The sensor primarily consists of magnetized plasma and two isotropic dielectrics with a periodic asymmetric structure. Due to the introduction of evanescent waves, a sharp peak in the transmittance spectrum can be calculated by the transmission matrix method, relying on which physical quantities such as plasma density, incidence angle, magnetic induction strength, etc. can be attained, and the refractive index can also be derived after the addition of dielectrics in the structure. After adjustment, the sensitivity and quality factor values of these physical quantities at the forward and backward propagation of electromagnetic waves are $1.027 \times 10^2$ $(2\pi c/d)^{-1} \cdot m^3$, $0.945 \times 10^2$ $(2\pi c/d)^{-1} \cdot m^3$, $1926.66$, $1772.05$, $0.00355$ $(2\pi c/d) \cdot degree^{-1}$, $0.01029$ $(2\pi c/d) \cdot degree^{-1}$, $378.03$, $1163.76$, $1.455 \times 10^{11} T^{-1}$, $1.014 \times 10^{11} T^{-1}$, $2235.02$, $3686.81$, $0.21309$ $(2\pi c/d) \cdot RIU^{-1}$, $0.09713$ $(2\pi c/d) \cdot RIU^{-1}$, $352.66$, $720.31$, respectively, where c is the speed of light in vacuum, and *d* is the thickness of one period structure of the proposed cylindrical photonic crystals.

| | | Magnetic induction | Plasma denisity | Refractive index | Incident angle |
|---|---|---|---|---|---|
| Forward propagation | S | $1.454 \times 10^{10}$ $T^{-1}$ | $1.027 \times 10^2$ $(2\pi c/d)^{-1} \cdot m^3$ | $0.21309$ $(2\pi c/d) \cdot RIU^{-1}$ | $0.00355$ $(2\pi c/d) \cdot degree^{-1}$ |
| | Q | $2235.02$ | $1926.66$ | $378.03$ | $352.66$ |
| Backward propagation | S | $1.014 \times 10^{10}$ $T^{-1}$ | $0.945 \times 10^2$ $(2\pi c/d)^{-1} \cdot m^3$ | $0.09713$ $(2\pi c/d) \cdot RIU^{-1}$ | $0.01029$ $(2\pi c/d) \cdot degree^{-1}$ |
| | Q | $3686.81$ | $1772.05$ | $1163.76$ | $720.63$ |

Dielectric A
Dielectric B
Magnetized Plasma

**Index Terms**—Cylindrical photonic crystals, magnetized plasma, nonreciprocity, evanescent wave, multiphysics sensor.
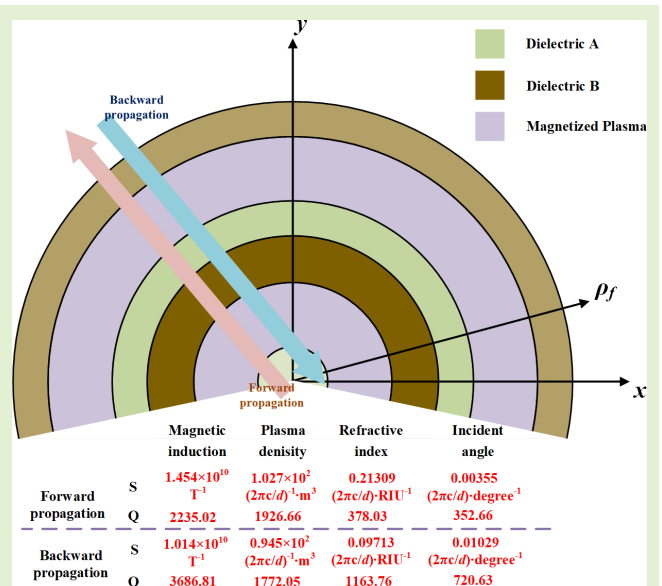
## I. INTRODUCTION

**T**HE superiority of the sensor [1]–[3] is mainly measured by the sensitivity (S), quality factor (Q), the figure of merit (FOM), and other indicators. The design of sensors with higher sensitivity, Q, and FOM has been the relentless pursuit of researchers. Among them, it has been put forward that photonic crystals (PCs) [4]–[6] could serve as the core structure of optical sensors for several years. Owing to the variety of excellent optical properties of PCs and the benefits of the simple structure together with the flexible design and the small size, they have launched a considerable impact on traditional sensors. On the one hand, the one-dimensional (1D)

plane PC, as a relatively simple and classical idealized model, is widely used in the design of various types of sensors and has a well-established technology. On the other hand, in pursuit of higher practicality and convenience, PCs sensors have the use of spherical photonic crystals (SPCs) [7]–[9] structures as the ultimate goal. However, the lack of theoretical formulations for the optical transport properties in SPCs has made this research very scarce and demanding. As a trade-off, the cylindrical photonic crystals (CPCs) [10]–[15] model, which is both practical and well-formulated theoretically, serves as a good transition between the two phases. There is a growing trend for a number of teams to shift their research focus to CPCs. Applying the principle of the transfer matrix method (TMM) [16], the formula applicable to the CPCs [17] can be obtained by expanding it on the column coordinate system.

Magnetized plasma [18], [19] is a typical kind of anisotropic dielectric whose dielectric constant can be controlled by the external magnetic field strength, plasma density, collision frequency, and other factors. In this work, the cylindrical magnetized plasma PCs (CMPPCs) [20] are designed with a peri-

TABLE I
COMPARISON OF METRICS BETWEEN DIFFERENT SENSORS*

| Reference | Basic Structure | | magnetic induction | plasma density | refractive index | Incidence angle |
|---|---|---|---|---|---|---|
| [27] | 1D PCs | L | $0 \sim$ infinite | none | none | none |
| | | Q | 7602 | | | |
| | | S | 6.5 nm·T⁻¹ | | | |
| | | FOM | 5.5 nm·T⁻¹ | | | |
| [28] | 1D PCs | L | none | none | $1.00026 \sim 1.00046$ | none |
| | | Q | | | 4000 | |
| | | S | | | $1.9 \times 10^5$ nm·RIU⁻¹ | |
| | | FOM | | | $3.6 \times 10^5$ RIU⁻¹ | |
| [29] | 1D PCs | L | none | none | $2 \sim 2.7$ | $25 \sim 70$ degrees |
| | | Q | | | / | / |
| | | S | | | 32.3 THz·RIU | 0.5 THz·degree⁻¹ |
| | | FOM | | | 100 RIU⁻¹ | 1.2 degree⁻¹ |
| This work | 1D CMPPCs | L | $0.644 \sim 2.361$ T | $1.789 \times 10^{19} \sim 4.472 \times 10^{19}$ m⁻³ | $1.2 \sim 2.2$ | $20 \sim 36$ degrees |
| | | Q | 3686.81 | 1926.66 | 720.31 | 1163.76 |
| | | S | $1.454 \times 10^{12}$ T⁻¹ | $5.448 \times 10^{-14}$ m³ | $4.017 \times 10^{10}$ RIU⁻¹ | $1.940 \times 10^9$ degree⁻¹ |
| | | FOM | $3.369 \times 10^4$ T⁻¹ | $8.976 \times 10^{-22}$ m³ | 168.17 RIU⁻¹ | 25.85 degree⁻¹ |

*The thickness of one period is defined as 10 mm here; linear range, quality factor, sensitivity and figure of merit are denoted by L, Q, S and FOM, respectively.

odic structure consisting of magnetized plasma and generally isotropic dielectrics, and the characteristics of columnar wave transmitting under TM polarization are discussed. At the same time, the proposed structure has significant nonreciprocal properties [21]–[23] due to the use of asymmetric arrays and the magneto-optical effects produced by the introduced magnetized plasma, which makes it possible for a sensor to perform measurements on two scales, simultaneously.

Additionally, the existence of evanescent waves [24]–[26] in the PCs, which cannot propagate in monolayer dielectrics, is a very substantial phenomenon. When the electromagnetic waves propagate from an optically dense medium to an optically sparse medium, total reflection occurs whenever the incidence angle is greater than the critical angle. Periodic CMPPCs act here as the equivalent of a resonant cavity, where the electromagnetic waves of a specific frequency incident at a specific angle can be made to pass nearly loss-free, i.e., exhibiting one or several sharp fronts in the transmission spectrum by adjusting parameters of the structure. Therefore, a sensor based on the evanescent wave principle will have a particularly high Q, this work is further designed based on the same. The evanescent wave principle can also be used in the design of optical switches, optical isolators, comb filters, and other devices.

In this work, we use the structure of nonreciprocal CMPPCs and apply the principle of evanescent waves to design a sensor. The superposition of multiple theories allows this sensor to have a larger linear range and a higher Q with multiple physical measurements. Very little work has been done in this area in existing studies. Table.I lists the metrics of the sensors designed by other researchers compared with this work.

## II. THEORETICAL MODEL

As shown in Fig.1, the structure of CMPPCs designed in this paper consists of magnetized plasma and two other isotropic dielectrics A, B. The thickness and refractive index of A and B are denoted by $d_A, d_B, n_A, n_B$. Prisms made
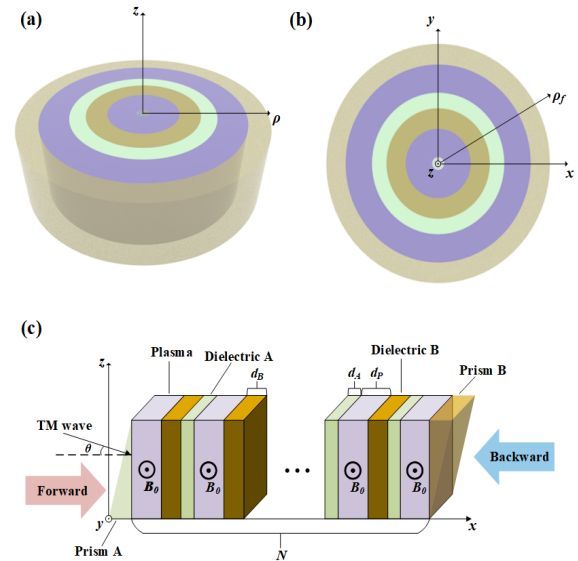


Fig. 1. The structure diagrams of the designed CMPPCs, (a) stereogram, (b) top view, and (c) cross-sectional view.

of the two dielectrics make up the innermost and outermost layers, respectively. To compose the structure of the $(APB)^N$, the magnetized plasma layers are added between the two dielectrics with a thickness of $d_p$, and the thickness of one period is $d = d_A + d_B + d_p$. It is worth mentioning that the structures (A)PB and AP(B), which consist of a prism and two other dielectric layers, are also considered as one period in this paper, and $N$ represents the number of periods of the whole structure. To ensure that the external magnetic field remains orthogonal to the wave vector, assume that the applied magnetic field is along the $\phi$-axis and is fixed as $B_0$. The electromagnetic wave is incident vertically at angle $\theta$ from the prism.

When a magnetic field is added, the dielectric constant of the magnetized plasma exhibits anisotropy and has the

following form in the columnar coordinate system [17]:

$$\varepsilon_p = \begin{bmatrix} \varepsilon_1 & j\varepsilon_2 & 0 \\ -j\varepsilon_2 & \varepsilon_1 & 0 \\ 0 & 0 & \varepsilon_3 \end{bmatrix} \tag{1}$$

where

$$\varepsilon_1 = 1 - \frac{\omega_p^2 (\omega + j v_c)}{\omega \left[ (\omega + j v_c)^2 - \omega_c^2 \right]} \tag{2}$$

$$\varepsilon_2 = \frac{-\omega_p^2 \omega_c}{\omega \left[ (\omega + j v_c)^2 - \omega_c^2 \right]} \tag{3}$$

$$\varepsilon_3 = 1 - \frac{\omega_p^2}{\omega (\omega + j v_c)} \tag{4}$$

plasma frequency $\omega_p = \sqrt{e^2 n_e / \varepsilon_0 m}$, cyclotron frequency of electron $\omega_c = e B_0 / m$, and $\omega$ is the angular frequency of the incident wave, $v_c$ is the collision frequency, $n_e$ is the plasma density, $B_0$ is the magnetic induction strength, the quantity and quality of the electron are represented by $e$ and $m$, respectively.

Firstly, starting with the set of Maxwell's equations for the TM wave incidence case, i.e., $E = e^{j\omega t}(E_\rho, E_\phi, 0)$ and $H = e^{j\omega t}(0, 0, H_z)$:

$$\nabla \times \mathbf{E} = -j\omega\mu_0 \mathbf{H} \tag{5}$$

$$\nabla \times \mathbf{H} = j\omega\varepsilon_0 \varepsilon_p \mathbf{E} \tag{6}$$

Neglecting the variation in the $z$-direction and removing the component that is constant to zero, the result of the above equation expanded in the column coordinate system can be expressed as

$$\frac{1}{\rho} \left[ \frac{\partial (\rho E_\phi)}{\partial \rho} - \frac{\partial E_\rho}{\partial \phi} \right] = -j\omega\mu_0 H_z \tag{7}$$

$$\frac{1}{\rho} \frac{\partial H_z}{\partial \phi} = j\omega\varepsilon_0 (\varepsilon_1 E_\rho - j\varepsilon_2 E_\phi) \tag{8}$$

$$\frac{\partial H_z}{\partial \rho} = -j\omega\varepsilon_0 (\varepsilon_1 E_\phi + j\varepsilon_2 E_\rho) \tag{9}$$

After eliminating $E_\rho$ and $E_\phi$ with $H_z$, Eqs.(4)-(6) can be combined as

$$\frac{1}{\rho} \frac{1}{\omega\varepsilon_0(\varepsilon_1^2 - \varepsilon_2^2)} [j\varepsilon_1 \frac{\partial}{\partial\rho}\rho\frac{\partial H_z}{\partial\rho} - \varepsilon_2\frac{\partial}{\partial\rho}\frac{\partial H_z}{\partial\phi}$$
$$+ \varepsilon_2\frac{\partial}{\partial\phi}\frac{\partial H_z}{\partial\rho} + j\varepsilon_1\frac{1}{\rho}\frac{\partial}{\partial\phi}\frac{\partial H_z}{\partial\phi}] = -j\omega\mu_0 H_z \tag{10}$$

Eq.(7) can be solved by the separation of variables method as

$$H_z(\rho, \phi) = V(\rho)\Phi(\phi) = [A J_m(k\rho) + B Y_m(k\rho)] e^{j\omega\phi} \tag{11}$$

When the incident wave is incident at angle $\theta$, $k = \omega\sqrt{\mu_0\varepsilon_0\varepsilon_{TM}}\cos\theta$ and $\varepsilon_{TM} = \frac{\varepsilon_1^2 - \varepsilon_2^2}{\varepsilon_1}$, $J_m$ and $Y_m$ are the Bessel and Neumann functions with azimuthal mode $m$, respectively. Substituting this solution into Eq.(6) yields the result

$$\frac{1}{j\omega\varepsilon_0} \frac{\partial V}{\partial \rho} e^{j\omega\phi} = -j\omega\varepsilon_0 (\varepsilon_1 E_\phi + j\varepsilon_2 E_\rho) \tag{12}$$

Defining

$$-\frac{1}{j\omega\varepsilon_0} \frac{\partial V}{\partial \rho} e^{j\omega\phi} = U(\rho) e^{j\omega\phi} \tag{13}$$

Then the form of $U(\rho)$ can be easily calculated as

$$U(\rho) = jp A J_m'(k\rho) + jp B Y_m'(k\rho) \tag{14}$$

where $p = \sqrt{\frac{\mu_0}{\varepsilon_0\varepsilon_{TM}}}\cos\theta$. Clearly, the relationship between $U$ and $V$ corresponding to different radii $\rho$ in the same dielectric layer can be related by a second order transfer matrix $\mathbf{M}_n$ in the following form

$$\begin{bmatrix} V(\rho_n) \\ U(\rho_n) \end{bmatrix} = \mathbf{M}_n \begin{bmatrix} V(\rho_{n0}) \\ U(\rho_{n0}) \end{bmatrix} \tag{15}$$

Let $m_i 11, m_i 12, m_i 21$ and $m_i 22$ be the four elements of $\mathbf{M}_{ni}$, respectively, which can be specifically expressed as [17]

$$m_{i11} = \frac{\pi}{2} k_n \rho_{i0} \left[ Y_m'(k_n\rho_{i0}) J_m(k_n\rho_i) - J_m'(k_n\rho_{i0}) Y_m(k_n\rho_i) \right] \tag{16a}$$

$$m_{i12} = -j\frac{\pi}{2}\frac{k_n}{p_n}\rho_{i0} [Y_m(k_n\rho_i) J_m(k_n\rho_{i0}) - J_m(k_n\rho_i) Y_m(k_n\rho_{i0})] \tag{16b}$$

$$m_{i21} = -j\frac{\pi}{2}k_n p_n\rho_{i0} \left[ Y_m'(k_n\rho_{i0}) J_m'(k_n\rho_i) - J_m'(k_n\rho_{i0}) Y_m'(k_n\rho_i) \right] \tag{16c}$$

$$m_{i22} = \frac{\pi}{2}k_n\rho_{i0} \left[ Y_m'(k_n\rho_i) J_m(k_n\rho_{i0}) - J_m'(k_n\rho_i) Y_m(k_n\rho_{i0}) \right] \tag{16d}$$

where subscript $n$ is A, B or TM, $i = 1, 2, 3 \ldots$ Representing the number of layers, $\varepsilon_{A,B} = n_{A,B}^2$. According to the principle of TMM, the transmission matrix of the column wave at the forward incidence is

$$\mathbf{M}_{forward} = \mathbf{M}_{TM1}\mathbf{M}_{B2}\mathbf{M}_{A3}\mathbf{M}_{TM4}\mathbf{M}_{B5}$$
$$\cdots \mathbf{M}_{A(3N-3)}\mathbf{M}_{TM(3N-2)} \tag{17}$$

Similarly, the transmission matrix at the backward incidence can be calculated by the following equation

$$\mathbf{M}_{backard} = \mathbf{M}_{TM(3N-2)}\mathbf{M}_{A(3N-3)}$$
$$\cdots \mathbf{M}_{B5}\mathbf{M}_{TM4}\mathbf{M}_{A3}\mathbf{M}_{B2}\mathbf{M}_{TM1} \tag{18}$$

The transmission and reflection coefficients are expressed as (19) and (20), shown at the bottom of the next page, where $M'_1$, $M'_2$, $M'_3$ and $M'_4$ are elements of the inverse matrix of $\mathbf{M}_{forward}$ or $\mathbf{M}_{backward}$, the subscripts $i$ and $f$ refer to the incident surface and the exit surface, respectively. $H_m^1$ and $H_m^2$ are the first and the second Hankel functions. And

$$C_{ml}^{1,2} = \frac{H_m^{'1,2}(k_l\rho_l)}{H_m^{1,2}(k_l\rho_l)} \Big|_{(l=i, f)} \tag{21}$$

The reflectance $R$ and transmittance $T$ can be indicated by $r_d$ and $t_d$ as

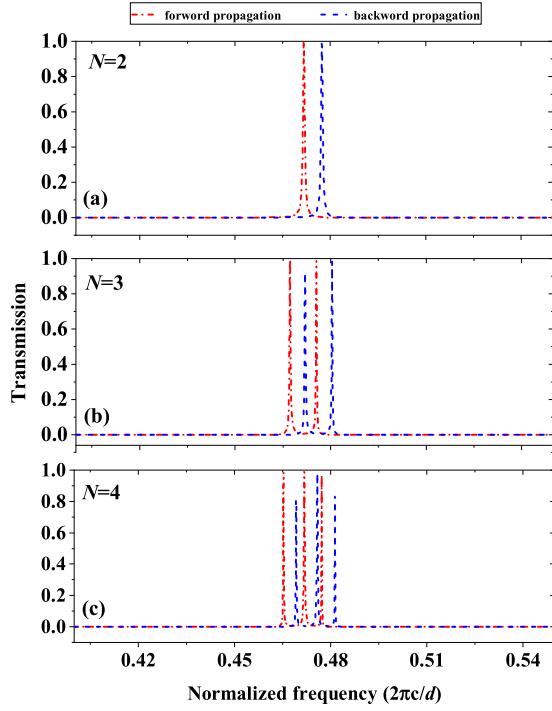$$R = |r_d|^2 \tag{22}$$

$$T = |t_d|^2 \tag{23}$$

**Fig. 2.** The transmission spectra with period number *N* between 2 and 4 and incidence angle $\theta$ of 30 degrees, (a) $N = 2$, (b) $N = 3$, and (c) $N = 4$.



**Fig. 3.** The transmission spectra at different plasma frequencies (a) the forward propagation, and (b) the backward propagation.

## III. ANALYSIS AND DISCUSSION

Adopting the structure of Fig.1, the initial parameters are $n_A = 2.8$, $n_B = 2.1$, $d_A = 0.24d$, $d_B = 0.32d$, $d_p = 0.44d$ and $d$ is set to the normalized length. As for the magnetized plasma, define $\omega_0 = 2\pi c/d$ as the normalized frequency, plasma frequency $\omega_p = \omega_0$, cyclotron frequency of electron $\omega_c = 1.2\omega_p$, collision frequency $v_c = 0.00001\omega_p$. The transmission spectra obtained for the number of periods N from 2 to 4 are given in Fig.2 at a 30 degrees incidence angle. Apparently, the number of transmission peaks depends on the number of periods $N$ for regular variation, which can be summarized as $N$-1 according to Fig.2. The difference $\Delta\omega_N(N = 2, 3, 4)$ between the forward and backward corresponding transmittable frequency points are 0.0056 ($2\pi c/d$), 0.0049 ($2\pi c/d$), and 0.0054 ($2\pi c/d$) respectively. The free spectral range (FSR) in the case of the forward (the subscript is expressed as FSRf) and backward (the subscript is expressed as FSRb) propagation for $N = 3$ is $\Delta\omega_{FSRf} = 0.01027$ ($2\pi c/d$) and $\Delta\omega_{FSRb} = 0.00852$ ($2\pi c/d$), which are calculated as $\Delta\omega_{FSRf1} = 0.00651$ ($2\pi c/d$), $\Delta\omega_{FSRf2} = 0.0541$ ($2\pi c/d$) for the forward transmission and $\Delta\omega_{FSRb1} = 0.00659$ ($2\pi c/d$), $\Delta\omega_{FSRb2} = 0.00551$ ($2\pi c/d$) for the backward
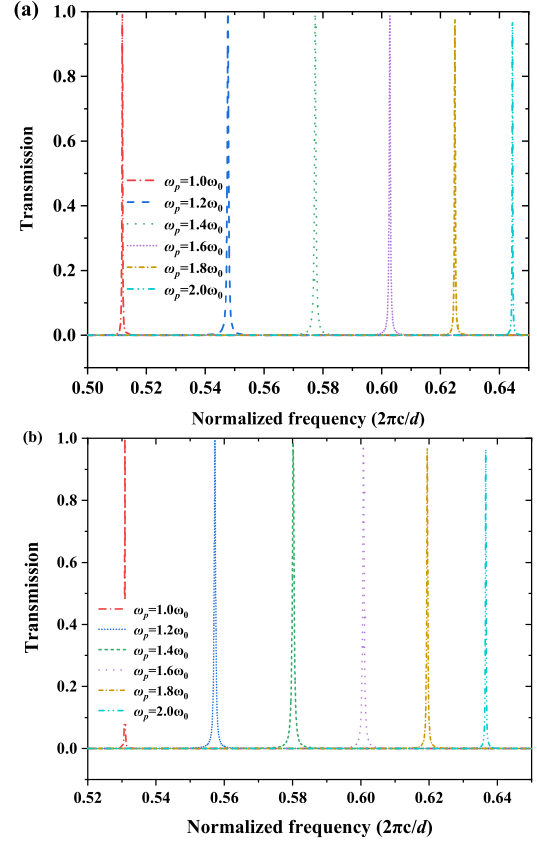
transmission at the case of 4 periods. To avoid crosstalk of multiple channels and to facilitate measurement, only the structure with a period number of 2 is used in the later work.

Next, we discuss the role of magnetized plasma parameters in regulating the position of the transmission frequency point, after parameter optimization, the refractive index of dielectric B ($n_B$) is 1.778, and other variables are the same as the initial data. Keeping the cyclotron frequency of electron $\omega_c$, collision frequency $v_c$ of the magnetized plasma constant to the multiplicity of the plasma frequency $\omega_p$, i.e., $\omega_c = 1.2\omega_p$ and $v_c = 0.00001\omega_p$, $\omega_p$ are taken as $\omega_0$, $1.2\omega_0$, $1.4\omega_0$, $1.6\omega_0$, $1.8\omega_0$, $2\omega_0$, and the transmission spectra of the forward and backward transmission are shown in Fig.3. With the gradual increase of $\omega_p$, the angular frequency corresponding to the transmission peak also increases significantly, from 0.51182 ($2\pi c/d$) at $\omega_p = \omega_0$ to 0.54771 ($2\pi c/d$), 0.57739 ($2\pi c/d$), 0.60275 ($2\pi c/d$), 0.62487 ($2\pi c/d$), 0.64444 ($2\pi c/d$) for the forward incidence, and from 0.53088 ($2\pi c/d$) to 0.55725 ($2\pi c/d$), 0.58019 ($2\pi c/d$), 0.60075 ($2\pi c/d$), 0.61945 ($2\pi c/d$),

$$r_d = \frac{(M_2' + jp_0C_{m0}^2M_1') - jp_fC_{mf}^2(M_4' + jp_0C_{m0}^2M_2')}{-(jp_0C_{m0}^1M_1' + M_3') + jp_fC_{mf}^2(jp_0C_{m0}^1M_2' + M_4')} \tag{19}$$

$$t_d = \frac{4\sqrt{\varepsilon_i/\mu_i}}{\pi K\rho_iH_m^2(k_i\rho_i)H_m^1(k_i\rho_i)[-(jp_iC_{mi}^1M_1' + M_3') + jp_fC_{mf}^2(jp_iC_{mi}^2M_2' + M_4')]} \tag{20}$$
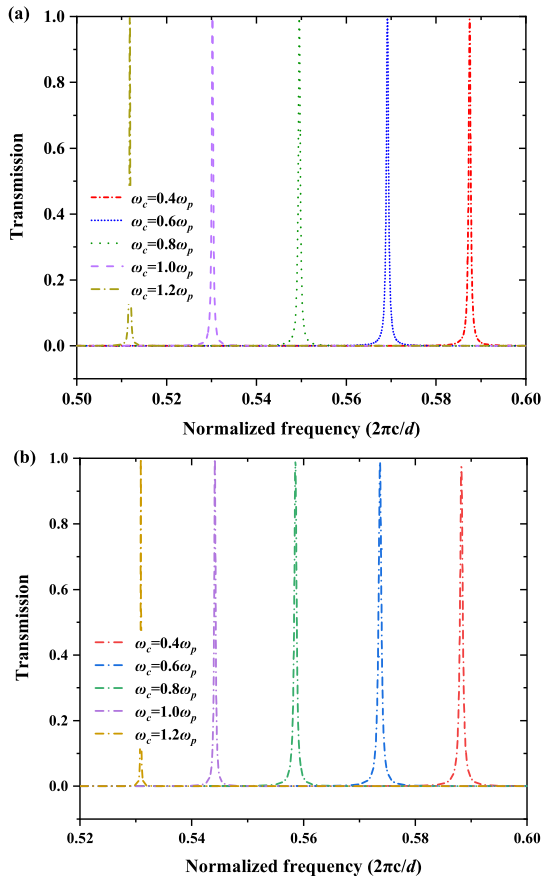
Fig. 4. The transmission spectra at different cyclotron frequency of electron (a) the forward propagation, and (b) the backward propagation.



Fig. 5. The magnetic field intensity distribution in the $z$-direction when the electromagnetic wave is incident at the frequency corresponding to the transmission peak at $\omega_p = \omega_0$, $\omega_c = 1.2\omega_p$ ($\omega = 0.5118$ ($2\pi c/d$)).



Fig. 6. (a) The transmission spectra of the forward and backward propagation at different magnetic induction strengths, and (b) the transmission spectra after linear fitting.

0.63657 ($2\pi c/d$) for the backward incidence. In both forward and backward transmission, the transmission peak attained at $\omega_p$ equal to 1 has the maximum Q, 2235.00 and 5104.58 were achieved, respectively.

Similarly, Fig.4 demonstrates the transmission spectra when the plasma frequency $\omega_p$ is fixed at $1.2\omega_0$ and the cyclotron frequency of electron $\omega_c$ increases regularly from $0.4\omega_p$ to $1.2\omega_p$. Unlike the results in Fig.3, the angular frequency of the transmission peak tends to decrease as $\omega_c$ increases. For the case of the forward propagation, the transmission peaks in Fig.4 are located at $\omega = 0.58748$ ($2\pi c/d$), $0.56917$ ($2\pi c/d$), $0.54955$ ($2\pi c/d$), $0.53021$ ($2\pi c/d$), $0.51182$ ($2\pi c/d$) and at $\omega = 0.58826$ ($2\pi c/d$), $0.57369$ ($2\pi c/d$), $0.55856$ ($2\pi c/d$), $0.54414$ ($2\pi c/d$), $0.53088$ ($2\pi c/d$) for the backward incidence. In addition, the transmission peak with $\omega_c = 1.2\omega_p$ has the highest transmittance (0.999006 and 0.999362 for the forward and backward incidence, respectively) and the narrowest half-height width compared to the others, which is to say that it has the highest Q (The results are the same as in the analysis of Fig.3), which will also contribute to the design of the sensor.

To demonstrate the existence of evanescent waves, the distributions of magnetic field intensity in the $z$-direction for TM waves incident at the frequency corresponding to the transmission peak at $\omega_p = \omega_0$, $\omega_c = 1.2\omega_p$ ($\omega = 0.5118$ ($2\pi c/d$)) are illustrated in Fig.5. For the case of the forward propagation, the evanescent wave is generated when the electromagnetic
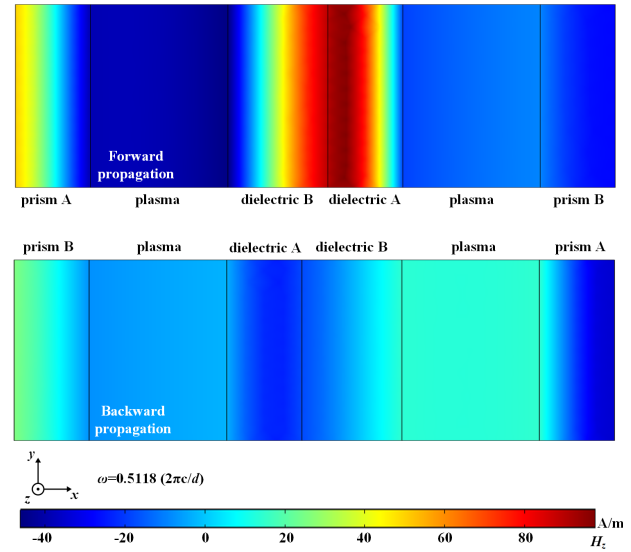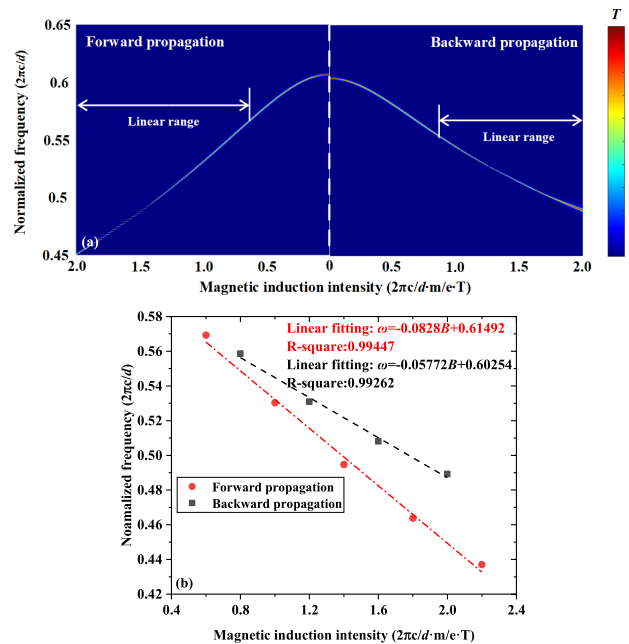
wave enters the magnetized plasma layer from prism A and passes through it due to its sufficiently thin thickness, and at the border of dielectric A and dielectric B with the magnetized plasma, total reflection occurs. As can be summarized in Fig.5, the electromagnetic field is intensely confined in dielectric A and dielectric B, which is working as a resonant cavity. The transmission peaks in the transmission spectrum are thus generated. In contrast, for the backward propagation case, the magnetic field's amplitude magnitude does not vary greatly across the structure, making it impossible to determine whether the magnetic field is contained.
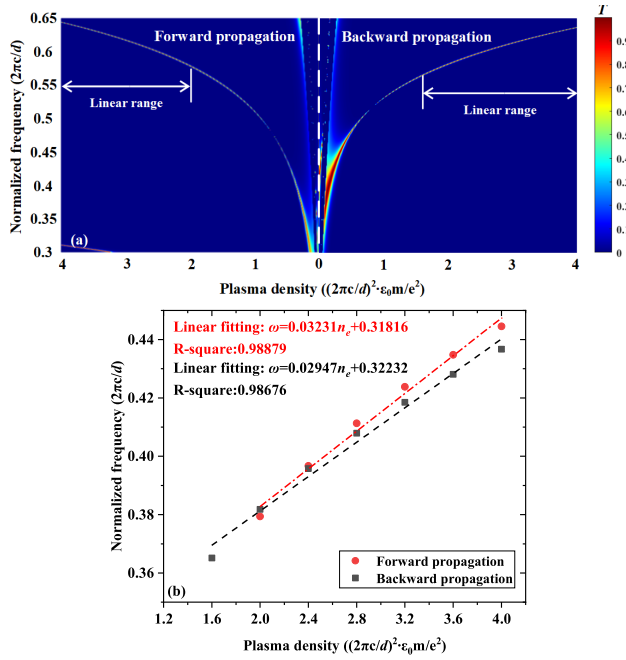
Fig. 7. (a) The transmission spectra of the forward and backward propagation at different plasma densities, and (b) the transmission spectra after linear fitting.
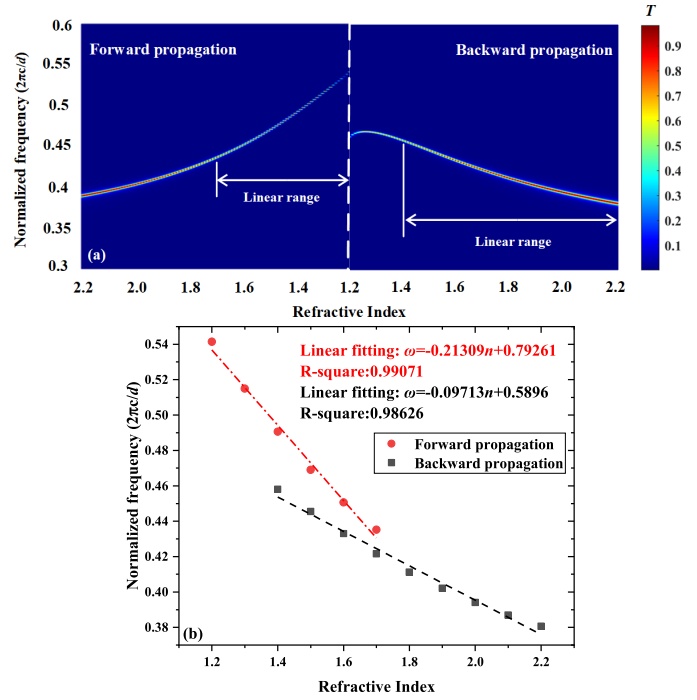


Fig. 8. (a) The transmission spectra of the forward and backward propagation at different refractive indices, and (b) the transmission spectra after linear fitting.

The sensor structure designed in this work allows for measurements of plasma density, magnetic induction strength, incidence angle and refractive index, etc. Since any tiny change in these external conditions will shift the position of the transmission peak within a certain range. Utilizing TMM, we discuss the measurement index of each physical quantity in this paper. The effective refractive index of the magnetized plasma may be changed by the intensity of the applied magnetic field, which also influences the position of the transmission peak, because $\omega_c$ is a function of the magnetic induction strength, which is the essential basis for the given sensor to measure the magnetic induction intensity. Fig.6(a) illustrates the transmission spectrum of the sensor at different magnetic induction strengths $B$. At the plasma frequency $\omega_p = \omega_0$, it can be observed that the linearity is high in the range of $B = 0.342 \times 10^{-12} \sim 1.252 \times 10^{-12} (2\pi c/d)\cdot$T for the forward propagation, which is $B = 0.455 \times 10^{-12} \sim 1.138 \times 10^{-12} (2\pi c/d)\cdot$T for backward propagation. The equations for the forward and backward propagation after linear fitting are $\omega = -0.0828B + 0.61492$ and $\omega = -0.05772B + 0.60254$. The R-square, which is used to indicate linearity, is as high as 0.99447 and 0.99262, respectively, confirming the reliability of the linear fit. In addition, for the forward propagation, $S_f = 1.454 \times 10^{10}$T$^{-1}$, $Q_f$ reaches 2235.02, and FOM$_f = 6.351 \times 10^{13} ((2\pi c/d)\cdot$T$)^{-1}$, the subscript f means the forward while the subscript b in the following indicates the backward. For the backward case, $S_b = 1.014 \times 10^{10}$T$^{-1}$, $Q_b = 3686.81$, and FOM$_b = 7.040 \times 10^{13} ((2\pi c/d)\cdot$T$)^{-1}$. These are high enough metrics for sensors.

In the same way as the magnetic induction intensity, the dependence of transmission peak frequency on the plasma density can be reflected by the plasma frequency, at the electron

cyclotron frequency $\omega_c = 1.2\omega_p$, the relationship between plasma density and structural transmittance is depicted in Fig.7. For sensing plasma density, the differentiation of the forward and backward propagation is relatively minor, the linear intervals are in the range of $n_e 6.293 \times 10^{-4} \sim 1.259 \times 10^{-3} (2\pi c/d)^2\cdot$m$^{-3}$ and $n_e = 5.034 \times 10^{-4} \sim 1.259 \times 10^{-3} (2\pi c/d)^2\cdot$m$^{-3}$, the linear fitting equations for the corresponding intervals are respectively $\omega = 0.03231n_e + 0.31816$ and $\omega = 0.02947n_e + 0.32232$ with R-square equal to 0.98676 and 0.98879. Although the R-square values of both linear fitted equations are below 0.99, they are still within the acceptable range. $S_f$ and $S_b$, as the forward and backward sensitivities, are equal to $1.027 \times 10^2 (2\pi c/d)^{-1}\cdot$m$^3$ and $0.945 \times 10^2 (2\pi c/d)^{-1}\cdot$m$^3$, with $Q_f = 1936.99$, $Q_b = 1772.05$ and FOM$_f = 3.189 \times 10^5 (2\pi c/d)^{-2}\cdot$m$^3$, FOM$_b = 2.684 \times 10^5 (2\pi c/d)^{-2}\cdot$m$^3$. From the fitted curves in Fig.7(b), it appears that the nonreciprocity of the forward and backward transport is not evident in the sensing of the plasma density. The linear range of the backward transmission is greater than the forward transmission, while the sensitivity value is slightly inferior.

Assuming that the dielectric to be measured is denoted by M, the structure of (A)PBMAP(B) can be formed after its insertion into the original structure, and the different refractive indices of the dielectric to be measured will also have an impact on the transmission spectrum. Based on this, plots of the refractive index measurement results are provided in Fig.8. When the thickness of the dielectric to be measured is set at $0.3d$, the linear interval of refractive index for the forward propagation is between 1.2 and 1.7 RIU, and the fitted equation is $\omega = -0.21309n + 0.79261$, which has an R-square
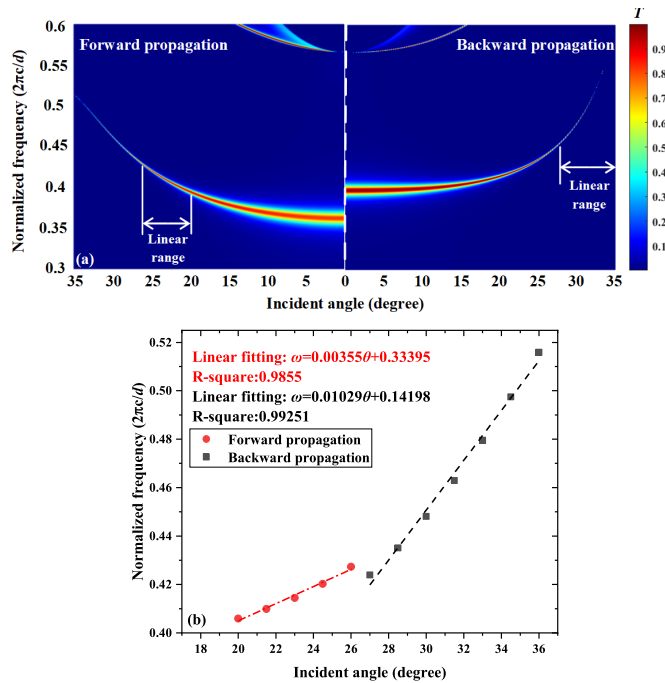
Fig. 9. (a) The transmission spectra of the forward and backward propagation at different incidence angles, and (b) the transmission spectra after linear fitting.

of 0.99071. The linear interval of the backward propagation is extended from 1.4 to 2.2 RIU, the relationship equation is $\omega = -0.09713n + 0.5896$, R-square equals 0.98626. Compared with the $S_f$ of 0.21309 $(2\pi c/d) \cdot RIU^{-1}$ for the forward propagation, the $S_b$ for backward propagation is merely 0.09713 $(2\pi c/d) \cdot RIU^{-1}$. $Q_f$ and $Q_b$ are 720.31 and 352.66, which are relatively poor indicators for the sensor. To $FOM_f$ and $FOM_b$ with values of 168.17 $RIU^{-1}$ and 148.62 $RIU^{-1}$. The measurement of the refractive index of the dielectric to be measured is subject to further optimization.

In addition, both the initial (A)PBAP(B) structure and the (A)PBMAP(B) structure with dielectric M inserted in the middle can measure the incidence angle, and Fig.9 displays diagrams of the results based on the (A)PBMAP(B) structure, where the refractive index of dielectric M is fixed at 1.7 and other conditions remain the same. When the incident angle is less than the critical angle of total reflection, the passband of the transmission spectrum is wide and the evanescent wave is almost non-existent. With the expansion of the angle, the passband becomes progressively narrower and the Q of the transmission peak increases significantly. In the linear interval of 20 to 26 degrees of the forward propagation, the fitted equation is $\omega = 0.00355\theta + 0.33395$ with an R-square of 0.9855. These data are 27 to 36 degrees for the backward propagation, $\omega = 0.01029\theta + 0.14198$, $R^2 = 0.99251$. For the forward propagation, $S_f = 0.00355$ $(2\pi c/d) \cdot degree^{-1}$, $Q_f = 378.03$ and $FOM_f = 3.10$ $degree^{-1}$, which are $S_b = 0.01029$ $(2\pi c/d) \cdot degree^{-1}$, $Q_f = 1163.76$ and $FOM_f = 25.85$ $degree^{-1}$ for the backward propagation.

It is worth noting that with the addition of the dielectric M to be measured, the symmetry of the structure is further broken,

and the nonreciprocal properties are more pronounced in the sensing for refractive index and angle of incidence compared to the structure without M. The fitted curve's sensitivity, R-squared, and Q, on the other hand, worsened. In the actual design, there is a trade-off between adding an additional layer of media to the structure or not.

## IV. CONCLUSION

In summary, in this work, a structure based on MCPCs, which can be used to measure several physical quantities such as the plasma density, refractive index magnetic, induction intensity, incidence angle, etc, is designed. The principle of evanescent waves is applied, and the nonreciprocal properties of the structure are further investigated. The $S_f$ of the four physical quantities measured by the transmission matrix method is calculated as magnetic induction strength: $1.455 \times 10^{11} T^{-1}$, plasma density: $1.027 \times 10^2$ $(2\pi c/d)^{-1} \cdot m^3$, refractive index: 0.21309 $(2\pi c/d) \cdot RIU^{-1}$ and incidence angle: 0.00355 $(2\pi c/d) \cdot degree^{-1}$ for the forward propagation of electromagnetic waves. $Q_f$ are 2235.03, 1926.66, 352.66, 378.03, respectively. For the backward propagation, $S_b$ and $Q_b$ are $1.014 \times 10^{11} T^{-1}$, $0.945 \times 10^2$ $(2\pi c/d)^{-1} \cdot m^3$, 0.09713 $(2\pi c/d) \cdot RIU^{-1}$, 0.01029 $(2\pi c/d) \cdot degree^{-1}$ and 3686.81, 1772.05, 720.31, 1163.76, respectively. This work promotes the application of magnetized plasma in the CPCs and provides new ideas for the design of CPCs-based sensors, which can be of application value with further parameter optimization.

## REFERENCES

[1] C. H. Ho, S. H. Lin, H. C. Hu, and Y. F. Tsay, "CHL1 functions as a nitrate sensor in plants," *Cell*, vol. 138, no. 6, pp. 1184–1194, 2009.

[2] W. Wu and Z. Zhang, "Defect-engineered $TiO_2$ nanotube photonic crystals for the fabrication of near-infrared photoelectrochemical sensor," *J. Mater. Chem. B*, vol. 5, no. 25, pp. 4883–4889, 2017.

[3] N. Ozana et al., "Noncontact speckle-based optical sensor for detection of glucose concentration using magneto-optic effect," *J. Biomed. Opt.*, vol. 21, no. 6, p. 065001, Jun. 2016.

[4] M. N. Romodina, I. V. Soboleva, A. I. Musorin, Y. Nakamura, M. Inoue, and A. A. Fedyanin, "Bloch-surface-wave-induced Fano resonance in magnetophotonic crystals," *Phys. Rev. B, Condens. Matter*, vol. 96, no. 8, Aug. 2017, Art. no. 081401.

[5] N. Malkova and C. Z. Ning, "Shockley and Tamm surface states in photonic crystals," *Phys. Rev. B, Condens. Matter*, vol. 73, no. 11, pp. 249–261, Mar. 2006.

[6] S. A. Skirlo, L. Lu, Y. Igarashi, Q. Yan, J. Joannopoulos, and M. Soljačić, "Experimental observation of large Chern numbers in photonic crystals," *Phys. Rev. Lett.*, vol. 115, no. 25, Dec. 2015, Art. no. 253901.

[7] C. Xiong, J. Zhao, L. Wang, H. Geng, H. Xu, and Y. Li, "Trace detection of homologues and isomers based on hollow mesoporous silica sphere photonic crystals," *Mater. Horizons*, vol. 4, no. 5, pp. 862–868, 2017.

[8] M. S. Thijssen et al., "Inhibited light propagation and broadband reflection in photonic air-sphere crystals," *Phys. Rev. Lett.*, vol. 83, no. 14, pp. 2730–2733, Oct. 1999.

[9] K. Zhong et al., "Fabrication of optomicrofluidics for real-time bioassays based on hollow sphere colloidal photonic crystals with wettability patterns," *J. Mater. Chem. C*, vol. 4, no. 33, pp. 7853–7858, 2016.

[10] Q.-Y. Wang, P.-X. Wang, B.-F. Wan, Y. Ma, and H.-F. Zhang, "Study on the nonreciprocal absorption properties of cylindrical photonic crystals embedded in graphene cascaded by periodic and Rudin–Shapiro sequences at large incident angles," *J. Appl. Phys.*, vol. 129, no. 22, Jun. 2021, Art. no. 223107.

[11] S. A. El-Naggar, "Optical guidance in cylindrical photonic crystals," *Optik*, vol. 130, pp. 584–588, Feb. 2017.

[12] S. A. El-Naggar, "Properties of defect modes in cylindrical photonic crystals," *Optik*, vol. 200, Jan. 2020, Art. no. 163447.

[13] Z. X. Wu, W. C. Li, E. D. Gu, and L. F. Wang, "Characteristics of 2D cylindrical photonic crystals band gap with square lattice," *Adv. Mater. Res.*, vols. 712–715, no. 1, pp. 302–305, 2013.

[14] S. A. El-Naggar, "Photonic gaps in one dimensional cylindrical photonic crystal that incorporates single negative materials," *Eur. Phys. J. D*, vol. 71, no. 1, p. 11, Jan. 2017.

[15] C. A. Hu, S. L. Yang, and T. J. Yang, "Switchable tunneling mode for cylindrical photonic quantum well consisting of photonic crystals containing liquid crystal," *Opt. Commun.*, vol. 297, pp. 141–146, Jun. 2013.

[16] Z.-Y. Li, "Principles of the plane-wave transfer-matrix method for photonic crystals," *Sci. Technol. Adv. Mater.*, vol. 6, no. 7, pp. 837–841, Jan. 2005.

[17] C.-A. Hu, C.-J. Wu, T.-J. Yang, and S.-L. Yang, "Analysis of optical properties in cylindrical dielectric photonic crystal," *Opt. Commun.*, vol. 291, pp. 424–434, Mar. 2013.

[18] H. F. Zhang, S. B. Liu, and B. X. Li, "Investigation on the properties of omnidirectional photonic band gaps in two-dimensional plasma photonic crystals," *Phys. Plasmas*, vol. 23, no. 1, p. 2486, 2016.

[19] C. Li, B. Guo, M. X. Gao, L. Peng, and X. Cai, "Negative refraction in plasma photonic crystals at below plasma frequency," *Optik*, vol. 127, no. 4, pp. 2308–2311, Feb. 2016.

[20] Q. Wang, P. Wang, B. Wan, and H. Zhang, "Investigation on the non-reciprocal properties of one-dimensional cylindrical magnetized plasma photonic crystals," *J. Opt. Soc. Amer. A, Opt. Image Sci.*, vol. 38, no. 6, p. 897, 2021.

[21] C. He *et al.*, "Nonreciprocal resonant transmission/reflection based on a one-dimensional photonic crystal adjacent to the magneto-optical metal film," *Opt. Exp.*, vol. 21, pp. 28933–28940, 2013.

[22] A. H. Gevorgyan and S. S. Golik, "Band structure peculiarities of magnetic photonic crystals," *J. Magn. Magn. Mater.*, vol. 439, pp. 320–327, Oct. 2017.

[23] S. R. Entezar and M. K. Habil, "Nonreciprocal optical isolation via graphene based photonic crystals," *J. Magn. Magn. Mater.*, vol. 449, pp. 33–39, Mar. 2018.

[24] Y.-T. Fang and Z.-C. Liang, "Unusual transmission through usual one-dimensional photonic crystal in the presence of evanescent wave," *Opt. Commun.*, vol. 283, no. 10, pp. 2102–2108, May 2010.

[25] E. Eremina, Y. Eremin, N. Grishina, and T. Wriedt, "Analysis of light scattering in the evanescent waves area by a cylindrical nanohole in a noble-metal film," *Opt. Commun.*, vol. 281, no. 13, pp. 3581–3586, Jul. 2008.

[26] D. Felbacq and R. Smaali, "Bloch modes dressed by evanescent waves and the generalized Goos–Hänchen effect in photonic crystals," *Phys. Rev. Lett.*, vol. 92, no. 19, May 2004, Art. no. 193902.

[27] D. Su, S. Pu, L. Mao, Z. Wang, and K. Qian, "A photonic crystal magnetic field sensor using a shoulder-coupled resonant cavity infiltrated with magnetic fluid," *Sensors*, vol. 16, no. 12, p. 2157, Dec. 2016.

[28] Z. A. Zaky, A. M. Ahmed, A. S. Shalaby, and A. H. Aly, "Refractive index gas sensor based on the Tamm state in a one-dimensional photonic crystal: Theoretical optimisation," *Sci. Rep.*, vol. 10, no. 1, p. 9736, Dec. 2020.

[29] B.-F. Wan, Y. Xu, Z.-W. Zhou, D. Zhang, and H.-F. Zhang, "Theoretical investigation of a sensor based on one-dimensional photonic crystals to measure four physical quantities," *IEEE Sensors J.*, vol. 21, no. 3, pp. 2846–2853, Feb. 2021.

**Jia-Tao Zhang** was born in Jiangsu, China, in 2001. He is pursuing the degree with the Nanjing University of Posts and Telecommunications, Nanjing, China. He engages in the research of cylindrical photonic crystals.

**Si-Si Rao** was born in Hubei, China, in 2001. She is currently pursuing the degree with the Nanjing University of Posts and Telecommunications. Nanjing, China, and mainly investigating nonlinear photonic crystals and evanescent wave.

**Hai-Feng Zhang** was born in Jiangxi, China, in 1978. He received the M.Sc. degree in electronics science and technology from Nanchang University, Nanchang, China, in 2008, and the Ph.D. degree from the College of Electronic and Information Engineering, Nanjing University of Aeronautics and Astronautics, Nanjing, China, in 2014.

He is working as a Professor at the College of Electronic and Optical Engineering & College of Flexible Electronics, Nanjing University of Posts and Telecommunications, Nanjing. His main research interests include the computational electromagnetics, plasma photonic crystals, plasma stealthy, and the electromagnetic properties of metamaterials.